High-pressure behavior of iron carbide (Fe_7C_3) at inner core conditions

Mainak Mookherjee,[1] Yoichi Nakajima,[1] Gerd Steinle-Neumann,[1] Konstantin Glazyrin,[1] Xiang Wu,[1,2] Leonid Dubrovinsky,[1] Catherine McCammon,[1] and Aleksandr Chumakov[3]

Received 1 July 2010; revised 29 October 2010; accepted 14 January 2011; published 1 April 2011.

[1] Carbon is a plausible light element candidate in the Earth's core owing to its cosmic abundance and its chemical affinity for iron. Recent experimental studies on Fe-C phase relations at high pressures have demonstrated that Fe_7C_3 iron carbide is a likely candidate for the Earth's inner core. Using electronic structure calculations, we determine the equation of state, the full elastic constant tensor, and the sound wave velocities for Fe_7C_3, up to inner core pressures. We find that Fe_7C_3 is ferromagnetic (*fm*) at low pressure, and that its compression behavior is well represented by a third-order Birch Murnaghan finite strain expression with V_0^{fm} = 9.1 Å^3/atom, K_0^{fm} = 231 GPa, and K'^{fm}_0 = 4.4. Under compression the magnetic moments of the Fe atoms gradually decrease, and at ~67 GPa the magnetic moment is lost. The high-pressure nonmagnetic phase (*nm*) has distinct finite strain parameters with V_0^{nm} = 8.8 Å^3/atom, K_0^{nm} = 291 GPa, and K'^{nm}_0 = 4.5. Calculated elastic constants show softening associated with the loss of magnetization. In addition, we have conducted nuclear resonant inelastic X-ray scattering experiments on ^{57}Fe enriched Fe_7C_3 at 1 bar and 300 K. On the basis of our nuclear resonant inelastic X-ray scattering spectra we have derived a Debye sound velocity of 3.18 km/s. The experimentally determined value is in good agreement with the computational predictions, based on athermal single elastic constants. The static *P* wave velocity at inner core pressures agrees well with seismological constraints, whereas the *S* wave velocity is greater by 30%. On the basis of the density of Fe_7C_3 at inner core conditions, we predict that the maximum possible carbon content of the inner core is around 1.5 wt %.

Citation: Mookherjee, M., Y. Nakajima, G. Steinle-Neumann, K. Glazyrin, X. Wu, L. Dubrovinsky, C. McCammon, and A. Chumakov (2011), High-pressure behavior of iron carbide (Fe_7C_3) at inner core conditions, *J. Geophys. Res.*, *116*, B04201, doi:10.1029/2010JB007819.

1. Introduction

[2] The Earth's core is significantly denser than the overlying mantle and consists of a metallic liquid outer core and a coexisting solid inner core that has been freezing out of the outer core through Earth's history [*Jacobs*, 1953]. From cosmochemical and geochemical arguments, there is a consensus in the Earth and planetary sciences community that the core is composed primarily of iron (Fe). Comparison of seismological data with experimental measurements on the compressibility of Fe shows that the Earth's outer core is lighter than pure iron by 5–10% and the inner core is lighter than solid iron by 3–7% (the so-called density deficit of the core) [*Birch*, 1964; *Brown and McQueen*, 1986; *Jephcoat and Olson*, 1987]. The density deficit of the core requires the presence of lighter elements [*Stevenson*, 1981], the nature of which has been the subject of extensive reviews in geochemistry [*McDonough*, 2003; *Li and Fei*, 2003] and geophysics [*Stixrude et al.*, 1997; *Badro et al.*, 2007] where many light elements have been identified as potential candidates and trade-offs are discussed. In exploring the various possibilities, it is to be noted that the light element should readily alloy with iron and be cosmochemically abundant. With these constraints, S, O, Si, C and H have been the most preferred candidates [*Hillgren et al.*, 2000].

[3] Distribution of carbon in various reservoirs of the Earth has been extensively researched, and there is little doubt that the solid Earth is the most important reservoir [*Javoy et al.*, 1982; *Sleep and Zahnle*, 2001]. However, the relative distribution between the metallic core and the silicate mantle is poorly understood.

[4] Some models of the carbon budget for the solid Earth [*Sleep and Zahnle*, 2001; *Coltice et al.*, 2004] do not include carbon in the Earth's core. On the other extreme, *Kuramoto* [1997] proposed complete partitioning of carbon to the core, based on thermodynamic models of gas solubilities in silicate and metallic melts. Geochemical arguments suggest that

[1]Bayerisches Geoinstitut, Universität Bayreuth, Bayreuth, Germany.
[2]School of Earth and Space Sciences, Peking University, Beijing, China.
[3]ID18 Nuclear Resonance Group, European Synchrotron Radiation Facility, Grenoble Cedex, France.

0148-0227/11/2010JB007819

carbon is one of the light alloying elements [*Wood*, 1993; *Poirier*, 1994; *Li and Fei*, 2003; *Huang et al.*, 2005] with concentration as high as 4 wt % [*Hillgren et al.*, 2000] and as low as 0.2 wt % [*McDonough*, 2003]. If carbon were the dominant light element in the core, then the core would have an orders of magnitude higher carbon budget than the mantle. If carbon were a minor light element, the contribution of the core to the total terrestrial carbon budget would be comparable to or smaller than that of the mantle [*Dasgupta and Walker*, 2008; *Dasgupta and Hirschmann*, 2010].

[5] Cosmochemically, less than 3×10^{-4} wt % of C is expected to be present in Fe condensed from the solar nebula, owing to a large difference in the condensation temperatures of C (<600 K) and Fe (~1470 K) at 10^{-3} atm [*Morgan and Anders*, 1980; *Anderson*, 2007]. In addition, C might have been partially lost owing to high-temperature processes during or after accretion [*Hillgren et al.*, 2000].

[6] Nevertheless, carbon is abundant with 3.6 wt % in carbonaceous chondrites (CI) [*Anderson*, 2007], and at the slightly elevated pressures (0.01–5.00 GPa) prevalent during planetary accretion and differentiation, the solubility of C in Fe is significantly enhanced based on the persistence of a eutectic point in the Fe-C systems up to 12 GPa as determined experimentally [*Hirayama et al.*, 1993] and in thermodynamic calculations [*Wood*, 1993]. The importance of such high-pressure processes is highlighted by the widespread occurrences of graphite and carbides in iron meteorites [*Wasson*, 1985]. Slow cooling rates on the order 0.4–4°C Ma^{-1} in many of these meteorites as determined by Widmanstätten textures [*Goldstein and Short*, 1967b, 1967a] indicate that the graphite and carbide-bearing iron meteorites are fragments of cores from planetesimals with radii of at least 100–400 km. Iron-based carbides, in the form of cohenite $(Fe,Ni)_3C$, which is similar in structure to cementite Fe_3C, have been observed in such meteorites [*Brett*, 1966; *Wasson*, 1985].

[7] On the basis of the extrapolation of thermodynamic data to inner core conditions, *Wood* [1993] proposed Fe_3C (6.7 wt % carbon) as an ideal inner core candidate, coexisting with pure Fe, as also observed in recent experiments [*Tateno et al.*, 2010]. This notion found support in ab initio computations that predicted the stability of coexisting Fe and Fe_3C over C dissolved in Fe [*Huang et al.*, 2005]. However, the proposed presence of Fe_3C has been questioned from two different angles: the elastic properties of Fe_3C at pressures of the Earth's core [*Vočadlo et al.*, 2002], and phase equilibria studies in the Fe-C binary system at pressures above 130 GPa [*Lord et al.*, 2009].

[8] On the basis of systematics of compressibility in intermetallic phases, *Wood* [1993] assumed a bulk modulus $K_0 = 174$ GPa and its pressure derivative $K_0' = 5.1$ for Fe_3C. X-ray diffraction studies on the equation of state of Fe_3C up to 73 GPa [*Scott et al.*, 2001] and 30 GPa [*Li et al.*, 2002] were in agreement with the parameters used by *Wood* [1993], but subsequent ab initio simulations by *Vočadlo et al.* [2002] revealed a magnetic transition (high-spin low-spin transition) at ~60 GPa that had a strong effect on the thermoelastic properties of Fe_3C at core pressures. In this study the high-pressure nonmagnetic phase was found to be substantially stiffer ($K_0 = 316$ GPa) than the previously measured bulk moduli [*Scott et al.*, 2001; *Li et al.*, 2002]. The experiments were restricted to conditions below or near the predicted transition pressures and were insensitive to magnetism. The choice of a low-bulk modulus by *Wood* [1993] led to an inaccurate extrapolation of phase equilibria at pressures relevant to inner core.

[9] In addition, the Fe-C phase diagram has been revisited and extended to higher pressures. On the basis of density measurements of liquid Fe_3C up to 9.5 GPa, *Terasaki et al.* [2010] concluded that carbon is likely to be partitioned into the solid phase, which for the Earth implies the inner core. *Nakajima et al.* [2009] conducted multianvil quench experiments to 14 GPa and in situ X-ray diffraction up to 29 GPa. They observed a new phase with Fe_7C_3 stoichiometry as a stable liquidus phase above 10 GPa, in contrast to the previously assumed Fe_3C cementite phase. *Lord et al.* [2009] recently extended the pressure range for phase equilibria studies in the Fe-C system to 70 GPa using the laser heated diamond anvil cell technique, and concluded that Fe_7C_3 is the liquidus phase up to core pressures. The occurrence of Fe_7C_3 as the liquidus phase in the ternary system Fe-C-S [*Dasgupta et al.*, 2009] further strengthens the importance of this phase for the core of the Earth and other planets.

[10] With Fe_7C_3 as a potential inner core phase, its thermoelastic parameters at inner core pressures are of geophysical and geochemical interest. In this article we determine the full elastic constant tensor of Fe_7C_3 at high pressure from first principles electronic structure simulations. Similar to the behavior of Fe_3C under compression, the possibility of a high-spin low-spin transition can have a significant effect on elastic parameters of Fe_7C_3. Hence we examine the behavior of both the magnetic and nonmagnetic phases of Fe_7C_3 at high pressure.

2. Method

2.1. Electronic Structure Method

[11] The electronic structure and energetics of the iron carbide Fe_7C_3 have been calculated with a density functional theory (DFT) based method [*Kohn and Sham*, 1965]. DFT describes the electronic structure of materials through the electron density, translating the solution for the many body wave function and associated energies to a number of one electron problems in the Kohn-Sham equations [*Kohn and Sham*, 1965]. The DFT solution for the energies in the system considered is exact in principle, but the nature of the electronic many-body interaction is mapped onto a potential for exchange and correlation that needs to be approximated. Here we have used the generalized gradient approximation (GGA-PBE) [*Perdew et al.*, 1996] that has been shown to yield good results for transition metals [*Steinle-Neumann et al.*, 1999; *Alfè et al.*, 2002b; *Steinle-Neumann et al.*, 2004; *Steinle-Neumann*, 2008] and some of its alloys [*Skorodumova et al.*, 2004; *Isaev et al.*, 2007; *Cote et al.*, 2008], including iron carbides [*Vočadlo et al.*, 2002; *Huang et al.*, 2005]. The electronic structure of the Fe-carbides is different from transition metal oxides and silicates [*Cococcioni and de Gironcoli*, 2005; *Alfredsson et al.*, 2004] for which standard approximations to exchange and correlation fail because of very localized electronic states, and theory beyond DFT has to be applied to accurately describe their properties [*Kolorenč and Mitas*, 2008;

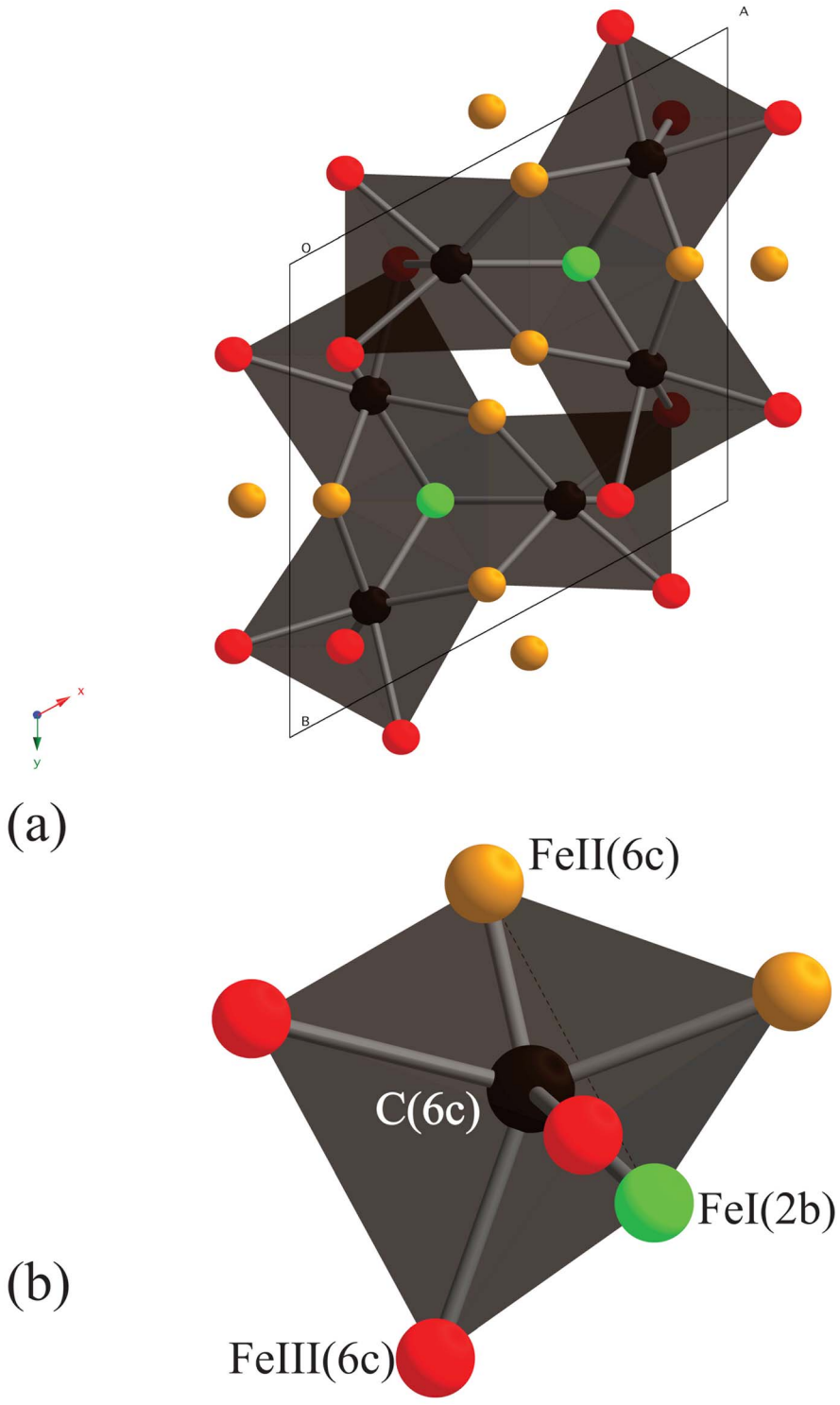

Figure 1. (a) Crystal structure of Fe_7C_3 with hexagonal symmetry, $P6_3mc$. (b) The iron atoms form a ditrigonal prism around the central carbon atom (black). Three such prisms are combined in a triangular arrangement. There are three distinct Fe sites: FeI (Wykcoff site 2b, green), FeII (Wykcoff site 6c, golden), and FeIII (Wykcoff site 6c, red). There is only one site for the carbon atom, C (Wykcoff site 6c). Each ditrigonal prism has three FeIII atoms, two FeII atoms, and one FeI atom. The FeI atom is located at the center of the triangle as shown in Figure 1a.

Kuneš et al., 2009]. Here we use the highly accurate projector augmented wave method (PAW) [*Kresse and Joubert*, 1999] as implemented in the Vienna ab initio simulation package (VASP) [*Kresse and Hafner*, 1993; *Kresse and Furthmuller*, 1996] which uses a plane wave basis set. We include plane waves up to cutoff energy (E_{cut}) of 1000 eV for the expansion of the charge density and the GGA-PBE atomic files provided within the VASP package [*Kresse and Joubert*, 1999].

[12] The crystal structure of the iron carbide Fe_7C_3 (Eckstrom-Adcock carbide) has hexagonal $P6_3mc$ space group (186) [*Herbstein and Snyman*, 1964] and contains 20 atoms in the primitive unit cell (Figure 1). The number of reciprocal space vectors at which the Kohn-Sham equations are solved (k-points) was chosen as $4 \times 4 \times 4$ [*Monkhorst and Pack*, 1976], which translates to 12 k-points within the irreducible wedge of the Brillouin zone. In addition to relaxing the magnetic moment in spin-polarized calculations for the ferromagnetic (*fm*) structure and two ferrimagnetic arrangements of Fe_7C_3 (with an antiferromagnetic nature), nonmagnetic (*nm*) calculations were performed for the whole compression range to study the influence of magnetism on the elastic parameters. The ferrimagnetic phases were created with spin up on the FeI (Wykcoff site 2b, Figure 1) and FeIII (Wykcoff site 6c) sites and spin down on the FeII (Wykcoff site 6c) site (*afm*1), as well as spin up on the FeI and FeII sites and spin down on the FeIII sites (*afm*2).

[13] In order to determine the relative stability of Fe_7C_3 and Fe_3C we have also calculated the energetics of Fe_3C, Fe and C. Fe_3C has an orthorhombic space group *Pnma* with Z = 4 [*Fasiska and Jeffrey*, 1965; *Vočadlo et al.*, 2002]. The k-point mesh was chosen as $8 \times 8 \times 8$ [*Monkhorst and Pack*, 1976], resulting in 64 k-points within the irreducible wedge of the Brillouin zone. Hexagonal close packed (hcp) iron with space group $P6_3/mmc$ (Z = 2) is believed to be stable at inner core conditions [*Mao et al.*, 1990; *Hemley and Mao*, 2001; *Nguyen and Holmes*, 2004]. Above 0.7 GPa carbon adopts the diamond structure [*Bundy*, 1989] with space group $Fd\bar{3}m$ (Z = 8). Computations were performed for a $20 \times 20 \times 20$ k-point mesh for both hcp iron and diamond with 1100 and 220 k-points, respectively, within the irreducible wedge of the Brillouin zone. With the k-point and E_{cut} chosen, total energies were converged to within 1 meV/atom and stresses to within 0.1 GPa.

[14] Athermal elastic constants for Fe_7C_3 were determined for the *fm* and *nm* phases. Elastic constants were computed through the changes in the stress tensor ($\underline{\underline{\sigma}}$) with respect to applied strain ($\underline{\underline{\varepsilon}}$) [*Mookherjee and Steinle-Neumann*, 2009a, 2009b]. We first calculated the equilibrium and relaxed structure at a given volume, V. Then we strained the lattice and let the internal degree of freedom of the crystal structure relax consistent with the symmetry. We applied positive and negative strains of magnitude $\delta = 1\%$ in order to accurately determine the stress in the appropriate limit of zero strain. The strained lattice $\vec{a}'$ is related to the unstrained lattice $\vec{a}$ by $\vec{a}' = (\underline{\underline{I}} + \underline{\underline{\varepsilon}})\vec{a}$, where $\underline{\underline{I}}$ is the identity matrix. Four distinct strain tensors ε were applied: $\varepsilon_{11} = \delta$; $\varepsilon_{21} = \varepsilon_{12} = \delta$; $\varepsilon_{31} = \varepsilon_{13} = \delta$; $\varepsilon_{33} = \delta$ (all other entries of $\varepsilon_{ij} = 0$) on the hexagonal lattice. These resulted in five independent elastic constants, c_{11} (= c_{22}), c_{12}, c_{13} (= c_{23}), c_{33}, c_{44} (= c_{55}), with $c_{66} = \frac{1}{2}(c_{11} - c_{12})$ [*Nye*, 1985].

2.2. Nuclear Resonant X-Ray Inelastic Scattering

[15] Fe_7C_3 samples were synthesized from a powder mixture of iron and graphite with a atomic ratio of Fe:C = 2:1, with higher carbon content compared to the target stoichiometry. To obtain sufficient intensity in the phonon energy spectrum of the sample, iron was doped with 25 wt % of ^{57}Fe. The mixture was packed into an MgO capsule and equilibrated at 18 GPa and 1873 K for 3 h using a multianvil apparatus at Bayerisches Geoinstitut. The recovered sample consists of large homogeneous domains (>100 μm) of Fe_7C_3 as determined by scanning electron microprobe analysis with energy dispersive spectroscopy. The excess carbon was observed as diamond only at the surface of the MgO capsule. We carefully selected the large domains under the microscope for further experiments. Subsequent X-ray diffraction confirmed the Fe_7C_3 phase with hexagonal symmetry (a = 6.88 Å and c = 4.53 Å). Minor peaks of MgO were observed.

[16] Nuclear resonant inelastic X-ray scattering (NRXIS) experiments were performed at the ID18 beamline of the European Synchrotron Radiation Facility (ESRF), Grenoble, France. The focused X-ray beam was less than 10 mm in diameter and has an energy resolution of 1.0 meV. Two avalanche photodiode detectors (APD) were used to collect the inelastic scattering in directions perpendicular to the X-ray beam. The diameter of the sample was ~120 μm. The NRXIS spectra were collected over a range of −80 to 80 meV around the ^{57}Fe nuclear resonance energy of 14.4 keV in steps of 0.2 meV. The collection time was 4 h.

3. Results

3.1. Energetics

[17] In order to assess the relative stability of Fe_7C_3 and Fe_3C, we have considered the following reactions:

$$Fe_7C_3 + 2Fe \leftrightarrow 3Fe_3C \quad (1)$$

$$3Fe_7C_3 \leftrightarrow 7Fe_3C + 2C \quad (2)$$

Reactions (1) and (2) have different bulk composition with 6.7 and 8.4 wt % C, respectively. At pressures corresponding to inner core conditions, the Fe_7C_3, Fe_3C and Fe phases are nonmagnetic (see also section 3.2), and hence we have estimated the enthalpy based on the nonmagnetic energies at static conditions. For Fe we have considered the hcp phase as outlined above. At static conditions (T = 0 K) the free energy change associated with the reaction, $\Delta G = \Delta H - T\Delta S$, is equivalent to the enthalpy change, ($\Delta G = \Delta H$). For reaction (1) with 6.7 wt % C, we find that Fe_3C is energetically stable compared to a mixture of Fe and Fe_7C_3 at all pressures (Figure 2). This observation does not agree with the recent experimental findings conducted in the iron-carbon systems [*Dasgupta et al.*, 2009; *Lord et al.*, 2009; *Nakajima et al.*, 2009] where Fe_7C_3 is a stable liquidus phase at higher pressures. This discrepancy can be traced to the considerably stiffer bulk modulus computed for hcp iron compared to experiments (Table 1). The discrepancy between measured and computed values of K_0 is consistent with previous ab initio studies [*Vočadlo et al.*, 1997; *Steinle-Neumann et al.*, 1999].

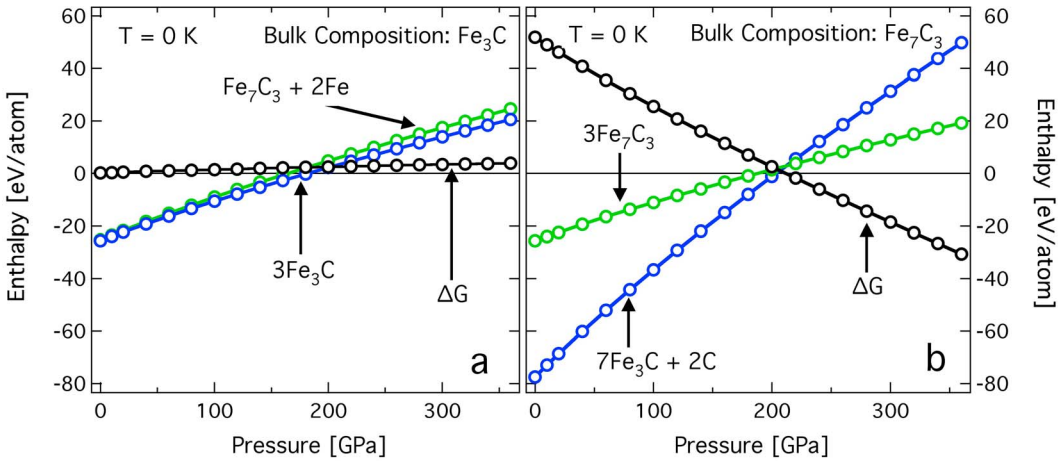

Figure 2. Energetics of the reaction (a) $Fe_7C_3 + 2Fe \leftrightarrow 3Fe_3C$ and (b) $3Fe_7C_3 \leftrightarrow 7Fe_3C + 2C$ at static conditions, T = 0 K. All calculations are for nonmagnetic phases. Note that for the bulk carbon content of 6.7 wt %, i.e., Figure 2a, the enthalpy of Fe_3C is lower than the mixture of Fe_7C_3 and Fe-hcp phase. With a bulk carbon content of 8.4 wt %, i.e., Figure 2b, the Fe_7C_3 phase is stabilized over Fe_3C and C-diamond at inner core conditions.

[18] For reaction (2) with bulk 8.4 wt % C, we find that Fe_3C and C (diamond) is the stable assemblage at lower pressure; however, above 200 GPa Fe_7C_3 is stabilized over Fe_3C and C. It is likely that temperature or other elements present in the core might affect the relative stability of Fe_7C_3 versus Fe_3C. The role of temperature could be examined by molecular dynamics simulations or by estimating the vibrational entropy through lattice dynamics. However, both

Table 1. Equation of State Parameters and Average Magnetic Moment (M) per Fe Atom in Atomic Units (μ_B), for Iron Carbides, Hexagonal Closed Packed (hcp) Iron, and Diamond[a]

Space Group	Phase	E_0 (eV/atom)	V_0 (cm^3/mol)	K_0 (GPa)	K′	M (μ_B)	Reference
				Fe_7C_3			
$P6_3mc$	nm	−8.53	52.82	291	4.5		this work (PBE-PAW)
		−8.54	52.35	339	4.0*		
	fm	−8.60	54.81	231	4.4	1.63	
		−8.60	54.79	238	4.0	1.63	
	afm1	−8.58	54.28	233	5.0	0.82	
		−8.58	54.41	243	4.0*	0.82	
	afm2	−8.57	53.99	223	6.0	0.04	
		−8.57	54.22	242	4.0*	0.04	
	exp.		55.47	253	3.6		Nakajima et al. (submitted manuscript, 2010)
				Fe_3C			
Pnma	nm	−8.50	21.58	298	4.6		this work (PBE-PAW)
		−8.51	21.54	329	4.0*		
			21.61	317	4.3		*Vocadlo et al.* [2002]
	fm	−8.59	22.92	223	3.1	1.92	this work (PBE-PAW)
		−8.59	22.93	211	4.0*	1.92	
			23.08	229	5.4	1.88	*Vocadlo et al.* [2002]
	exp.		23.37	175	5.2		*Scott et al.* [2001]
			23.38	174	4.8		*Li et al.* [2002]
				Fe (hcp)			
$P6_3mmc$	nm	−8.37	6.17	296	4.4		this work (PBE-PAW)
		−8.37	6.12	296	4.0*		
			5.90	292	4.4		*Steinle-Neumann et al.* [1999]
			6.26	290	4.0		*Vocadlo et al.* [1997]
	exp.		6.73	165	5.3		*Mao et al.* [1990]
			6.75	165	5.0		*Dewaele et al.* [2006]
				C (Diamond)			
Fd3m	comp.	−9.06	3.44	434	3.6		this work (PBE-PAW)
		−9.06	3.45	377	4.0*		
	exp.		3.41	446	3.0		*Occelli et al.* [2003]

[a]E_0, V_0, K_0, and K′ are zero pressure energy, volume, bulk modulus, and its pressure derivative, respectively. All computations were fit with a third- and second-order (K′ = 4.0, indicated by asterisk for fixed K′) Eulerian finite strain equation of state.

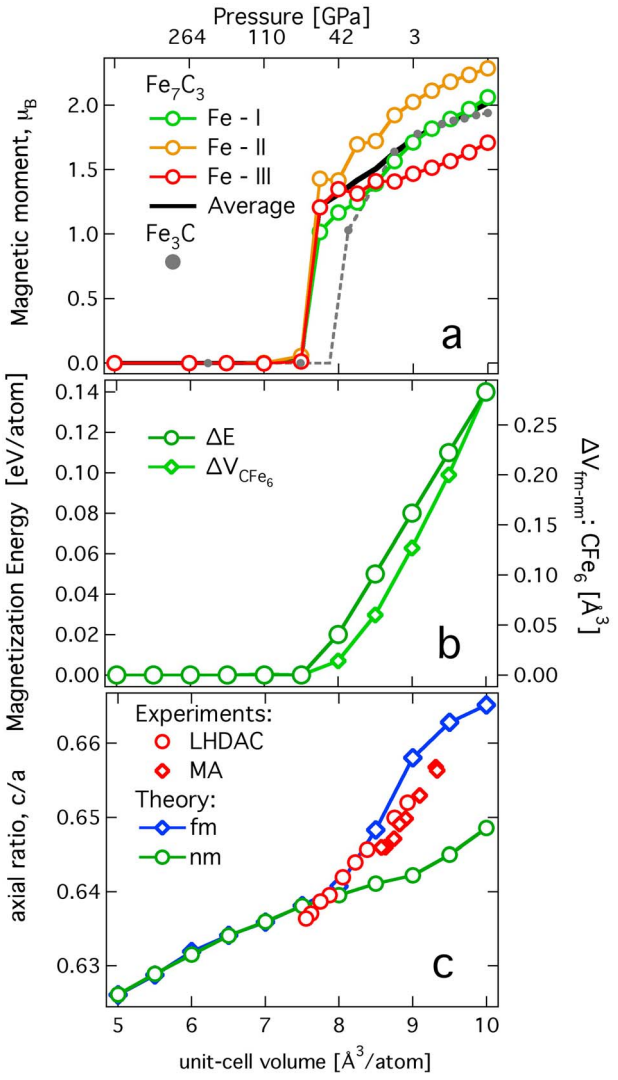

Figure 3. (a) Variation of magnetic moments for the ferromagnetic phase of Fe_7C_3 as a function of volume. Shown are values for FeI (green), FeII (golden), and FeIII (red). The black line shows the average magnetic moment, and the gray filled circles and dashed line show the average magnetic moment of Fe_3C [*Vočadlo et al.*, 2002]. The magnetic moments collapse at 7.5 Å^3/atom for Fe_7C_3. (b) Magnetization energy, i.e., the energetic difference between the magnetic and nonmagnetic phases at the same volume, for Fe_7C_3 also vanishes at 7.5 Å^3/atom. The volume difference for the ditrigonal CFe_6 polyhedral units between the *fm* and *nm* phases are also shown in Figure 3b. (c) The *c*/*a* ratio for Fe_7C_3 for the ferromagnetic (*fm*, blue open rhomb and line) and nonmagnetic structures (*nm*, green open circle and line). Red open rhomb (laser heated diamond anvil cell) and open (multianvil, 300 K) circle are experimental data (Nakajima et al., submitted manuscript, 2010).

methods are rather expensive given the large and complex system in question, and it is beyond the scope of the current study.

[19] Nevertheless, with the experimental findings and the theoretical confirmation (for 8.4 wt % C bulk composition) that Fe_7C_3 is stable at high pressures and forms the liquidus phase [*Dasgupta et al.*, 2009; *Lord et al.*, 2009; *Nakajima et al.*, 2009], it is clearly worth exploring its physical properties using DFT-based computations.

3.2. Magnetism

[20] Ferromagnetic Fe_7C_3 is found to be energetically stable over both ferrimagnetic configurations (intermediate in energy) and over the nonmagnetic solution for all volumes larger than 7.5 Å^3/atom, where the magnetic moment is lost from the structure on all Fe sites and the magnetization energy drops to zero (Figure 3). The magnetic moment per Fe for the ferromagnetic phase is 1.63 μ_B at $V_0^{fm} \sim 9.1$ Å^3/atom (Table 1), with individual moments being 1.71 μ_B for FeI, 2.03 μ_B for FeII, and 1.47 μ_B for FeIII. For the *afm*1 and *afm*2 phases the net magnetic moments are 0.82 and 0.04 at V_0^{afm1} and V_0^{afm2}, respectively. They consist of 2.05 (1.21) μ_B for FeI, −0.42 (1.19) μ_B for FeII and 1.66 (−1.52) μ_B for FeIII in the *afm*1 (*afm*2) structures. In comparison, the average magnetic moment for Fe_3C based on theory and experiment at V_0^{fm} is 1.88 μ_B [*Vočadlo et al.*, 2002] and 1.72–1.78 μ_B [*Hofer and Cohn*, 1959; *Shabanova and Trapeznikov*, 1973].

[21] For Fe_7C_3, *Tsuzuki et al.* [1984] measured the magnetic moment to be 1.31 μ_B at ambient conditions, which is significantly lower than our calculations. A similar value of 1.35 μ_B for Fe_3C was reported in their study, which is also lower than that in previous studies. As pointed out by *Tajima and Hirano* [1990], lower values by *Tsuzuki et al.* [1984] may be caused by the imperfection in sample preparation. It is therefore necessary to reexamine the magnetic moment of Fe_7C_3.

[22] The pressure of magnetic collapse (67 GPa) is very similar to that of cementite Fe_3C predicted from DFT-based computations (~60 GPa) [*Vočadlo et al.*, 2002; *Ono and Mibe*, 2010]. This transition pressure corresponds to anomalous behavior in inelastic X-ray scattering dispersion above 68 GPa [*Fiquet et al.*, 2009]. However, high-pressure magnetic measurements indicate a lower transition pressure, although there is considerable discrepancy between different studies. A synchrotron Mössbauer spectroscopy study on Fe_3C implies a magnetic collapse between 4.3 and 6.5 GPa [*Gao et al.*, 2008]. X-ray circular dichroism measures loss of magnetism near 10 GPa [*Duman et al.*, 2005], and by X-ray emission spectroscopy the transition pressure is determined to be approximately 25 GPa [*Lin et al.*, 2004].

3.3. Equation of State and Structure Under Compression

[23] As mentioned above, the magnetization energy (ΔE_{nm-fm}) decreases linearly and vanishes at 7.5 Å^3/atom, i.e., at 67 GPa, in agreement with the magnetic collapse (Figure 3).

[24] In the volume range 10.5 to 7.5 Å^3/atom, i.e., the region where the *fm* solution is energetically favored, the *c*/*a* ratio in the *fm* phase is larger than that of the *nm* phase (Figure 3). As the structure is compressed, the *c*/*a* ratio for the *fm* phase is reduced and it approaches the *c*/*a* ratio for the *nm* phase. They become equal at 7.5 Å^3/atom, corresponding to the magnetic collapse (Figure 3). The predicted decrease in *c*/*a* for the *fm* phase is in good agreement with experimental measurements (Y. Nakajima et al., Thermo-

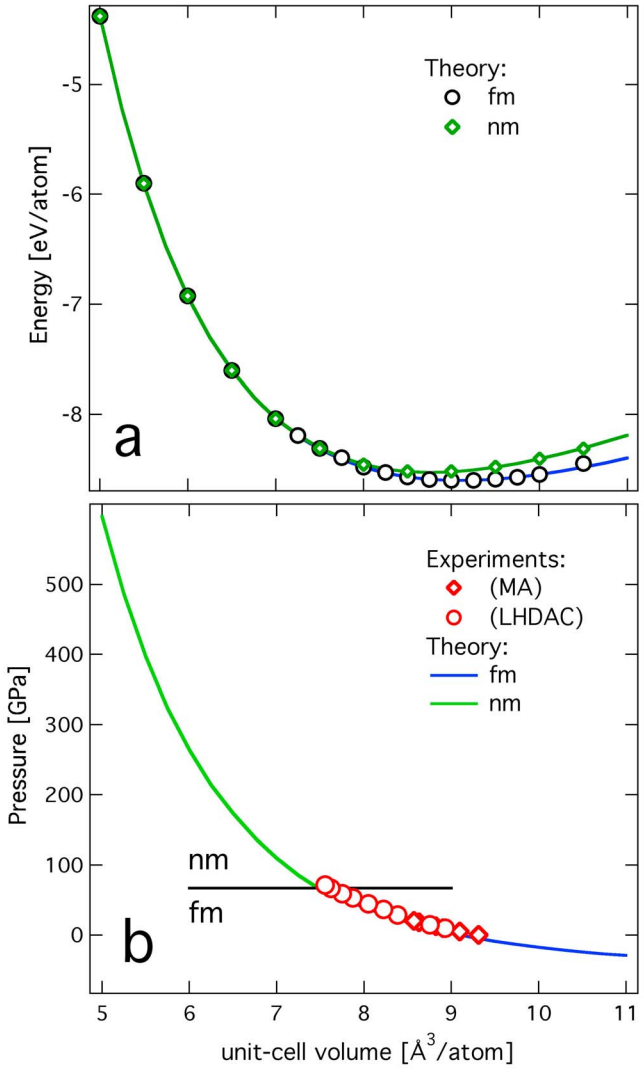

Figure 4. Energetics and equation of state of Fe_7C_3. (a) Plot of computed energy as a function of volume for the ferromagnetic (*fm*, black open circles) and nonmagnetic (*nm*, green open rhombs) phase. A finite strain fit to the computed *fm* energies between 10.5 and 7.75 Å^3/atom is shown by the blue line. The green line shows the finite strain fit to the *nm* energies. (b) Blue and green lines represent the computed P-V Birch Murnaghan equations of state for Fe_7C_3 at low and high pressure, respectively. Red symbols show data from laser heated diamond anvil cell experiments (open circles) and multianvil experiments at 300 K (open rhombs) from the work of Nakajima et al. (submitted manuscript, 2010).

elastic properties of Fe_7C_3: Implication for carbon in the Earth's inner core, submitted to *American Mineralogist*, 2010). As is the case for elemental cobalt [*Antonangeli et al.*, 2008], the *c*/*a* ratio appears to be a very sensitive indicator for the presence of magnetism at low pressure and its loss at high pressure.

[25] At 10 Å^3/atom the volume difference of the ditrigonal prism CFe_6 (Figure 1) between the *fm* and *nm* phases is around 0.3 Å^3. The volume differences decrease linearly upon compression and mimic the behavior of the magnetization energy (Figure 3).

[26] The calculated energy-volume relations for *fm* and *nm* Fe_7C_3 are shown in Figure 4. For the *fm* phase we find that a third-order Birch-Murnaghan finite strain equation of state (BM-EoS) [*Birch*, 1947] adequately describes energy-volume results between 10.5 and 7.75 Å^3/atom, with V_0^{fm} = 9.1 Å^3/atom, K_0^{fm} = 231 GPa and K'^{fm}_0 = 4.4. The energy-volume relationship for the *nm* phase between 10.5 and 5.0 Å^3/atom is described by BM-EoS parameters of V_0^{nm} = 8.77 Å^3/atom, K_0^{nm} = 291 GPa, and K'^{nm}_0 = 4.5 (Table 1). Similar to Fe_3C, there is a significant difference in the bulk moduli of the phases, with the *nm* Fe_7C_3 being considerably stiffer than the *fm* phase, as illustrated by the energy difference between the *nm* and *fm* E-V EoS (Figure 4).

3.4. Elasticity

[27] For both the *fm* and *nm* phases, the elastic constants increase upon compression. At 67 GPa, where magnetism collapses, an anomalous reduction for some of the elastic constants for the *fm* phase (c_{11}^{fm}, c_{12}^{fm} and c_{44}^{fm}, in Voigt notation c_{ij}) is predicted (Figure 5). Upon further compression, all the elastic constants increase monotonically. The elastic constants of the *nm* phase increase monotonically with pressure, merging with those of the *fm* phase after the loss of magnetism. Finite strain fits to the elasticity data (now in full fourth-rank tensor notation c_{ijkl}) were made using the formulation

$$c_{ijkl} = (1+2f)^{3.5}\left[c_{ijkl0} + b_1 f + 0.5 b_2 f^2\right] - P\Delta_{ijkl}, \quad (3)$$

where

$$f = 0.5\left[(V_0/V)^{2/3} - 1\right] \quad (4)$$

is the finite strain and

$$b_1 = 3K_0\left(c'_{ijkl0} + \Delta_{ijkl}\right) - 7c_{ijkl0}, \quad (5)$$

$$b_2 = 9K_0^2 c''_{ijkl0} + 3K'_0\left(b_1 + 7c_{ijkl0}\right) - 16b_1 - 49c_{ijkl0}, \quad (6)$$

$$\Delta_{ijkl} = -\delta_{ij}\delta_{kl} - \delta_{ik}\delta_{jl} - \delta_{il}\delta_{jk}. \quad (7)$$

c'_{ijkl0} and c''_{ijkl0} are the first and second derivatives of c_{ijkl} with respect to pressure. Δ_{ijkl} takes a value of −3 for longitudinal (c_{iiii} in full tensor and c_{ii} in Voigt notation, with i = 1, 2, 3) and off-diagonal elastic constants (c_{iijj} in full tensor and c_{ij} in Voigt notation, with i = 1, 2, 3, i ≠ j), −1 for shear constants (c_{ijij} in full tensor notation with i = 1,2,3, i ≠ j and c_{ij} in Voigt notation with i = 4, 5, 6, i = j), and 0 otherwise [*Stixrude and Lithgow-Bertelloni*, 2005]. At pressures below the magnetic collapse, $c_{11}^{nm} > c_{11}^{fm}$ and $c_{12}^{nm} > c_{12}^{fm}$, indicating that magnetism affects the [100] (and symmetrically equivalent [010]) direction in the Fe_7C_3 structure, making them softer than the values in the corresponding nonmagnetic structure. For the shear elastic constant $c_{44}^{fm} > c_{44}^{nm}$, i.e., the relationship between the *fm* and *nm* phases is opposite, indicating that aligned spins resist shearing. The dependent shear elastic constant, c_{66}^{fm} =

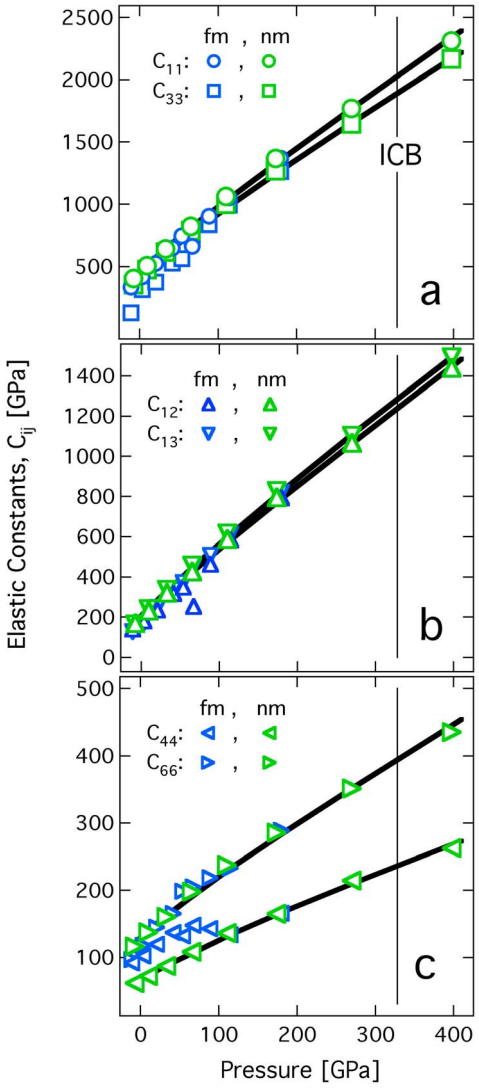

Figure 5. Single crystal elastic constants of Fe_7C_3 *fm* and *nm* phases as a function of pressure. (a) Longitudinal elastic constants: c_{11} (open circles) and c_{33} (open square); (b) off-diagonal elastic constants: c_{12} (upward pointing triangle) and c_{13} (downward pointing triangle). (c) Shear elastic constants: c_{44} (triangle pointing toward left) and c_{66} (triangle pointing toward right). Green symbols show the *nm* phase and blue symbols represent the *fm* phase. Lines are finite strain fits. Note that the *fm* elastic constants are lower than the *nm* elastic constants at low pressure except for c_{44} and c_{66}. Also, the elastic constants c_{11} and c_{12} of the magnetic phase exhibit softening at 67 GPa.

$0.5(c_{11}^{fm} - c_{12}^{fm})$, does not show this effect prominently and increases monotonically at all pressures.

[28] The isotropic bulk (K) and shear (G) moduli are determined using the relations

$$K_{Voigt} = (1/9)[2c_{11} + c_{33} + 2(c_{12} + 2c_{23})], \quad (8)$$

$$K_{Reuss} = [2s_{11} + s_{33} + 2(s_{12} + 2s_{23})]^{-1}, \quad (9)$$

$$G_{Voigt} = (1/15)[2c_{11} + c_{33} - (c_{12} + 2c_{23}) + 3(2c_{44} + c_{66})], \quad (10)$$

$$G_{Reuss} = 15[4(2s_{11} + s_{33} - (s_{12} + 2s_{23})) + 3(2s_{44} + s_{66})]^{-1}. \quad (11)$$

Here $s_{ijkl}(= c_{ijkl}^{-1})$ are the elastic compliances (inverse of the elastic constant tensor) and Voigt notation for the compliance tensor is used [*Oganov et al.*, 2002]. Hill averages (Table 2) are estimated as the average of Voigt and Reuss bounds. We compute

$$v_P = \sqrt{\frac{K + \frac{4}{3}G}{\rho}}, \quad v_S = \sqrt{\frac{G}{\rho}}, \quad (12)$$

with K and G the Hill averages of the bulk and shear modulus, respectively.

[29] The anomalies in the single crystal elastic constants (Figure 5) at the loss of magnetism are reflected in the aggregate moduli and sound velocities and, similar to studies in cobalt [*Goncharov et al.*, 2004; *Antonangeli et al.*, 2005; *Steinle-Neumann*, 2008], should be detectable by high-pressure techniques that can infer acoustic velocities such as inelastic X-ray scattering [*Antonangeli et al.*, 2005; *Fiquet et al.*, 2009] or impulsive stimulated light scattering [*Goncharov et al.*, 2004].

[30] In order to assess our computational results we have compared predictions with ambient NRXIS results at 1 bar and 300 K (Figure 6). The inelastic spectrum contains the information on the partial vibrational density of states (pDOS) of Fe in Fe_7C_3. The pDOS is related to the Debye velocity (v_D) by the following relation:

$$D(E) = \frac{\overline{m}}{2\pi^2\hbar^3\rho v_D^3}E^2, \quad (13)$$

Table 2. Elastic Constants c_{ij} (in Voigt Notation), Bulk (K) and Shear (G) Moduli for Fe_7C_3 at Zero Pressure Volume and Their Initial Pressure Derivative[a]

	Fe_7C_3 (*fm*) (This Study)		Fe_7C_3 (*nm*) (This Study)		Fe_3C[b]	Fe_3C[c]
[GPa]	M_0	M_0'	M_0	M_0'	M_0	M_0
C_{11}	397	5.7	458	5.9	394	417
C_{22}	397	5.7	458	5.9	412	416
C_{33}	247	8.6	425	5.7	360	381
C_{12}	173	3.1	200	3.7	157	157
C_{13}	168	3.9	205	3.9	146	171
C_{23}	168	3.9	205	3.9	166	174
C_{44}	102	3.1	67	0.7	83	82
C_{55}	102	3.1	67	0.7	133	136
C_{66}	112	3.3	129	3.0	136	140
K_{Hill}	223	4.7	301	4.4	233	227
G_{Hill}	102	1.3	87	1.0	115	75

[a]Zero pressure volume is represented by subscript zero; its initial pressure derivative is represented by prime.
[b]*Henriksson et al.* [2008].
[c]*Jiang et al.* [2008].

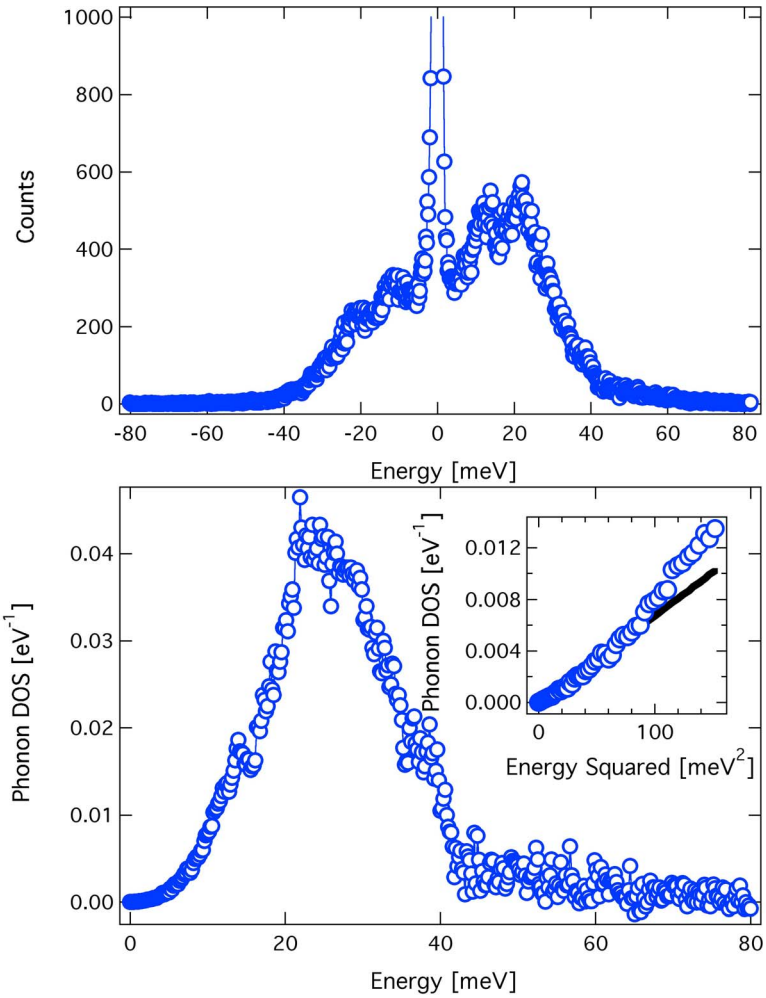

Figure 6. (a) NRXIS spectra of polycrystalline Fe_7C_3 at 1 bar and 300 K and (b) Fe partial phonon density of states pDOS of Fe_7C_3 extracted from NRXIS spectra at 1 bar and 300 K. The inset shows the plot of pDOS versus energy squared for low energies (<12 meV), exhibiting a linear relationship at energies between 0 and 100 meV^2. The linear relation is used to estimate the Debye velocity (v_D).

where ρ is the density of the material, and $\overline{m}$ is the mass of the nuclear resonant isotope [*Sturhahn and Jackson*, 2007]. The Debye velocity (v_D) is related to longitudinal (v_P) and shear wave velocity (v_S) by

$$\frac{3}{v_D^3} = \frac{1}{v_P^3} + \frac{2}{v_S^3}. \tag{14}$$

The experimentally determined density of polycrystalline Fe_7C_3 at ambient conditions is around 7.73 g/cm^3, and the corresponding v_D is 3.18 km/s. At the same density, the computed velocity is v_D = 3.97 km/s, ~20% greater than in experiments. This discrepancy could be associated with the thermal effects on the elastic constants and with the choice of the exchange and correlation potential. It is also important to note that small amounts of impurities in the synthesized samples could severely influence the observed v_D [*Sturhahn and Jackson*, 2007], similar to estimates of the magnetic moments [*Tajima and Hirano*, 1990].

4. Geophysical Significance

[31] In order to constrain the amount of iron carbide that could be present in the inner core, we need to evaluate its density at temperatures relevant for the inner core and combine the results with that of pure iron and then compare values to seismic reference models such as the preliminary reference Earth model (PREM) [*Dziewonski and Anderson*, 1981].

[32] The temperature of the Earth's core continues to be a subject of current research. Computations on the melting of iron and melting point depression due to the light element present in the core [*Alfè et al.*, 2002a], as well as relating high-pressure and high-temperature shear elasticity of iron to that of the inner core [*Steinle-Neumann et al.*, 2001], point to a temperature of ~5600–5700 K at the inner core

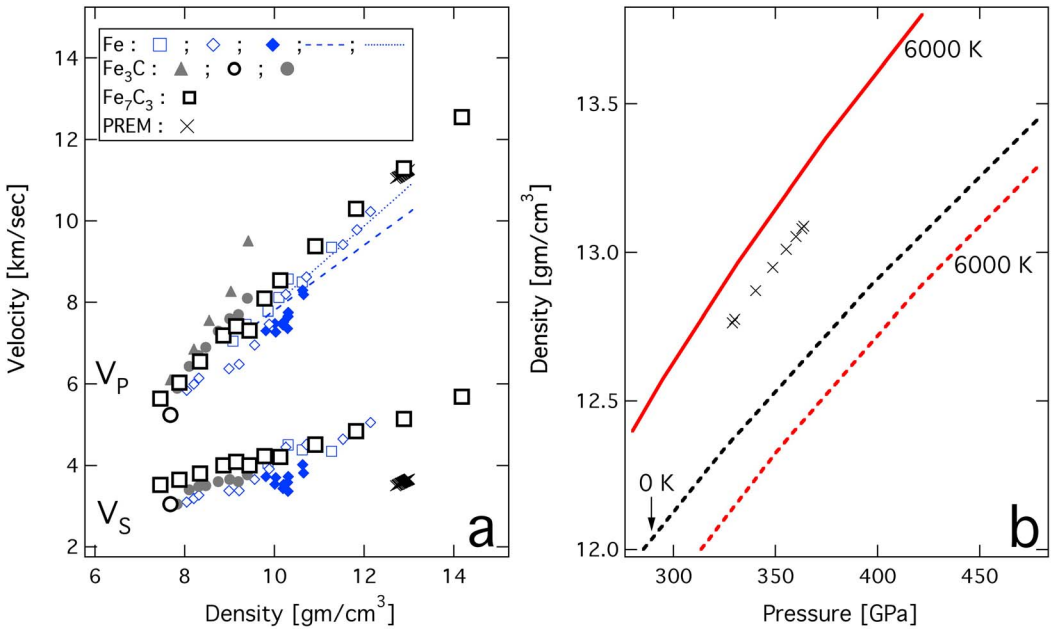

Figure 7. (a) Velocity-density systematics for iron and iron carbide alloys. Compressional wave velocity (v_P) and shear wave velocity (v_S) are plotted with respect to density for the ferromagnetic Fe_7C_3 phase (present study, black open squares). Note the softening of v_P and v_S at the transition from ferromagnetic to nonmagnetic phase at 67 GPa. Also shown are data for Fe_3C by *Gao et al.* [2008] with gray filled circles and by *Dodd et al.* [2003] in black open circles. Data on hcp-Fe at various temperatures are shown in blue symbols: [*Lin et al.*, 2005] (700–1700 K) with filled rhombs, [*Mao et al.*, 2001] (300 K) with open rhombs, [*Fiquet et al.*, 2001] (298 K) with dashed lines, [*Antonangeli et al.*, 2004] (300 K) with a blue open square, and along the Hugoniot [*Brown and McQueen*, 1986] with a dotted line. Large crosses show seismological values for the inner core from preliminary reference Earth model (PREM) [*Dziewonski and Anderson*, 1981]. (b) Densities of Fe_7C_3 (static black dashed line and 6000 K red dashed line) and hcp-Fe [*Isaak and Anderson*, 2003], (6000 K, solid red line). Large crosses show seismological values for the inner core from PREM [*Dziewonski and Anderson*, 1981].

boundary (ICB, 329 GPa). Experimental extrapolations of Fe melting curves to the ICB [*Brown and McQueen*, 1986; *Ma et al.*, 2004; *Nguyen and Holmes*, 2004], however, yield a temperature that is 500–1000 K lower.

[33] We extrapolate the computed density of Fe_7C_3 to the temperature range that is likely to cover inner core conditions with a Debye-Grüneisen model following *Mookherjee and Stixrude* [2009]. The zero-point pressure is given by

$$P_{zp} = \frac{9n\gamma k_B \theta_D}{8V}, \tag{15}$$

where θ_D is the Debye temperature, γ is the Grüneisen parameter, V is the volume of the unit cell, n is the number of atoms in the unit cell, and k_B is the Boltzmann constant. In the Debye approximation, the thermal energy is given by

$$E_{th} = 9nk_B\left(\frac{T}{\theta_D}\right)^3 T \int_0^{\theta_D/T} \left(x^3/(e^x - 1)\right)dx \tag{16}$$

and the thermal pressure is

$$P_{th} = \frac{\gamma E_{th}}{V}. \tag{17}$$

The volume dependence of γ and θ_D are approximated with the relations

$$\gamma(V) = \gamma_0\left(\frac{V}{V_0}\right)^q \tag{18}$$

$$\theta_D = \theta_0 \exp\left(\frac{\gamma_0 - \gamma(V)}{q}\right). \tag{19}$$

We determine $\theta_D \sim 920$ K, $\gamma_0 \sim 2.57$, and $q \sim 2.2$ on the basis of experimental data (Nakajima et al., submitted manuscript, 2010).

[34] The computed static P wave velocity agrees well with the reference Earth model while the calculated S wave velocity is considerably faster (by ~30%) than PREM (Figure 7). In comparison, the P and S wave velocities of Fe_3C, extrapolated to inner core conditions, are 14% and 25% greater, respectively [*Gao et al.*, 2008]. It is worth

noting that temperature is likely to reduce the seismic wave velocity by a few percent [*Lin et al.*, 2005], making the agreement of the *P* wave velocity worse and reducing the discrepancy between the *S* wave velocity and PREM [*Dziewonski and Anderson*, 1981]. Similarly, the difference of v_S for pure iron at high temperatures and the reference Earth model is pronounced, and a number of possible causes for the discrepancy between material properties and seismically observed shear wave velocity have been discussed. It could be related to nonlinear thermoelastic effects at core condition [*Steinle-Neumann et al.*, 2001], attenuation in the inner core with quality factor (Q) ~200–400 [*Souriau and Roudil*, 1995], or partial melting of around 3–10% [*Singh et al.*, 2000].

[35] As the presence of carbides has been predicted to be stable over the substitutional incorporation of C in the Fe lattice [*Huang et al.*, 2005], Fe_7C_3 is a plausible carbide phase for the inner core coexisting with Fe. As its extrapolated density is lower than that of the inner core [*Dziewonski and Anderson*, 1981; *Kennett et al.*, 1995], it can account for some of the density deficit (Figure 6). We determine the maximum volume fraction of Fe_7C_3 in the inner core at 6000 K and ICB pressure using the relation

$$\rho_{PREM} = x\rho_{Fe_7C_3} + (1-x)\rho_{Fe}. \quad (20)$$

With $\rho_{Fe} \sim 12.9$ g cm^{-3}, $\rho_{Fe_7C_3} \sim 12.1$ g cm^{-3}, and $\rho_{PREM} \sim 12.76$ g cm^{-3}, we find $x = 18$ vol % or a maximum possible carbon content of ~1.5 wt % in the inner core. This upper limit is a first-order approximation as the inner core might contain other volatiles as well [*Jephcoat and Olson*, 1987; *Stixrude et al.*, 1997], and the estimated carbon budget of the core varies between 4 wt % [*Hillgren et al.*, 2000] and 0.2 wt % [*McDonough*, 2003]. Also, the thermoelastic parameters that enter the thermal corrections are not well constrained at inner core conditions.

5. Conclusion

[36] In Fe_7C_3, magnetic collapse occurs at around 67 GPa and is associated with elastic softening in c_{11}, c_{12}, c_{44}. The magnetic collapse is correlated with changes in *c/a* ratio and reduction of the CFe_6-polyhedral volumes. The calculated *P* wave velocity is in good agreement with seismic models for the Earth's inner core, whereas the *S* wave velocity is larger by 30%. The predicted Debye velocity is also in good agreement with the experimentally determined Debye velocity using NRXIS at ambient conditions. The discrepancy in *S* wave velocity might be related to temperature-induced anelasticity or the presence of partial melts in the inner core. On the basis of the equation of state parameters for the nonmagnetic phase, which is predicted to be stable at pressure and temperature relevant for the inner core, the maximum carbon content in the inner core is likely not to exceed 1.5 wt %.

[37] **Acknowledgments.** We acknowledge the European Synchrotron Radiation Facility for providing the synchrotron radiation facilities. This project was partly supported by funds from the German Science Foundation (DFG) Priority Programs SPP1236 (CMC), SPP1488 (GSN), and the German Federal Ministry of Education and Research (BMBF).

References

Alfè, D., M. J. Gillan, and G. D. Price (2002a), Composition and temperature of the Earth's core constrained by combining ab initio calculations and seismic data, *Earth Planet. Sci. Lett.*, *195*(1–2), 91–98, doi:10.1016/S0012-821X(01)00568-4.

Alfè, D., G. D. Price, and M. J. Gillan (2002b), Iron under Earth's core conditions: Liquid-state thermodynamics and high-pressure melting curve from ab initio calculations, *Phys. Rev. B*, *65*(16), 165118, doi:10.1103/PhysRevB.65.165118.

Alfredsson, M., G. D. Price, C. R. A. Catlow, S. C. Parker, R. Orlando, and J. P. Brodholt (2004), Electronic structure of the antiferromagnetic *B*1-structured FeO, *Phys. Rev. B*, *70*(16), 165111, doi:10.1103/PhysRevB.70.165111.

Anderson, D. L. (2007), *New Theory of the Earth*, Cambridge Univ. Press, New York.

Antonangeli, D., F. Occelli, H. Requardt, J. Badro, G. Fiquet, and M. Krisch (2004), Elastic anisotropy in textured hcp-iron to 112 GPa from sound wave propagation measurements, *Earth Planet. Sci. Lett.*, *225*(1–2), 243–251, doi:10.1016/j.epsl.2004.06.004.

Antonangeli, D., M. Krisch, G. Fiquet, J. Badro, D. L. Farber, A. Bossak, and S. Merkel (2005), Aggregate and single-crystalline elasticity of hcp cobalt at high pressure, *Phys. Rev. B*, *72*(13), 134303, doi:10.1103/PhysRevB.72.134303.

Antonangeli, D., L. R. Benedetti, D. L. Farber, G. Steinle-Neumann, A. L. Auzende, J. Badro, M. Hanfland, and M. Krisch (2008), Anomalous pressure evolution of the axial ratio *c/a* in hcp cobalt: Interplay between structure, magnetism, and lattice dynamics, *Appl. Phys. Lett.*, *92*(11), 111911, doi:10.1063/1.2897038.

Badro, J., G. Fiquet, F. Guyot, E. Gregoryanz, F. Occelli, D. Antonangeli, and M. d'Astuto (2007), Effect of light elements on the sound velocities in solid iron: Implications for the composition of Earth's core, *Earth Planet. Sci. Lett.*, *254*(1–2), 233–238, doi:10.1016/j.epsl.2006.11.025.

Birch, F. (1947), Finite elastic strain of cubic crystals, *Phys. Rev.*, *71*(11), 809–824, doi:10.1103/PhysRev.71.809.

Birch, F. (1964), Density and composition of mantle and core, *J. Geophys. Res.*, *69*(20), 4377–4388, doi:10.1029/JZ069i020p04377.

Brett, R. (1966), Cohenite in meteorites: A proposed origin, *Science*, *153*(3731), 60–62, doi:10.1126/science.153.3731.60.

Brown, J. M., and R. G. McQueen (1986), Phase transitions, Grüneisen parameter, and elasticity for shocked iron between 77 GPa and 400 GPa, *J. Geophys. Res.*, *91*(B7), 7485–7494, doi:10.1029/JB091iB07p07485.

Bundy, F. P. (1989), Pressure-temperature phase diagram of elemental carbon, *Physica A*, *156*(1), 169–178, doi:10.1016/0378-4371(89)90115-5.

Cococcioni, M., and S. de Gironcoli (2005), Linear response approach to the calculation of the effective interaction parameters in the LDA+U method, *Phys. Rev. B*, *71*(3), 035105, doi:10.1103/PhysRevB.71.035105.

Coltice, N., L. Simon, and C. Lecuyer (2004), Carbon isotope cycle and mantle structure, *Geophys. Res. Lett.*, *31*, L05603, doi:10.1029/2003GL018873.

Cote, A. S., L. Vočadlo, and J. P. Brodholt (2008), The effect of silicon impurities on the phase diagram of iron and possible implications for the Earth's core structure, *J. Phys. Chem. Solids*, *69*(9), 2177–2181, doi:10.1016/j.jpcs.2008.03.031.

Dasgupta, R., and M. M. Hirschmann (2010), The deep carbon cycle and melting in Earth's interior, *Earth Planet. Sci. Lett.*, *298*, 1–13, doi:10.1016/j.epsl.2010.06.039.

Dasgupta, R., and D. Walker (2008), Carbon solubility in core melts in a shallow magma ocean environment and distribution of carbon between the Earth's core and the mantle, *Geochim. Cosmochim. Acta*, *72*(18), 4627–4641, doi:10.1016/j.gca.2008.06.023.

Dasgupta, R., A. Buono, G. Whelan, and D. Walker (2009), High-pressure melting relations in Fe-C-S systems: Implications for formation, evolution, and structure of metallic cores in planetary bodies, *Geochim. Cosmochim. Acta*, *73*(21), 6678–6691, doi:10.1016/j.gca.2009.08.001.

Dewaele, A., P. Loubeyre, F. Occelli, M. Mezouar, P. I. Dorogokupets, and M. Torrent (2006), Quasihydrostatic equation of state of iron above 2 Mbar, *Phys. Rev. Lett.*, *97*(21), 215504, doi:10.1103/PhysRevLett.97.215504.

Dodd, S. P., G. A. Saunders, M. Cankurtaran, B. James, and M. Acet (2003), Ultrasonic study of the temperature and hydrostatic-pressure dependences of the elastic properties of polycrystalline cementite (Fe_3C), *Phys. Status Solidi A*, *198*(2), 272–281, doi:10.1002/pssa.200306613.

Duman, E., M. Acet, E. F. Wassermann, J. P. Itie, F. Baudelet, O. Mathon, and S. Pascarelli (2005), Magnetic instabilities in Fe_3C cementite particles observed with FeK-edge X-ray circular dichroism under pressure, *Phys. Rev. Lett.*, *94*(7), 075502, doi:10.1103/PhysRevLett.94.075502.

Dziewonski, A. M., and D. L. Anderson (1981), Preliminary reference Earth model, *Phys. Earth Planet. Inter.*, *25*(4), 297–356, doi:10.1016/0031-9201(81)90046-7.

Fasiska, E. J., and G. A. Jeffrey (1965), On cementite structure, *Acta Crystallogr.*, *19*, 463–471, doi:10.1107/S0365110X65003602.

Fiquet, G., J. Badro, F. Guyot, H. Requardt, and M. Krisch (2001), Sound velocities in iron to 110 gigapascals, *Science*, *291*(5503), 468–471, doi:10.1126/science.291.5503.468.

Fiquet, G., J. Badro, E. Gregoryanz, Y. W. Fei, and F. Occelli (2009), Sound velocity in iron carbide (Fe_3C) at high pressure: Implications for the carbon content of the Earth's inner core, *Phys. Earth Planet. Inter.*, *172*(1–2), 125–129, doi:10.1016/j.pepi.2008.05.016.

Gao, L. L., et al. (2008), Pressure-induced magnetic transition and sound velocities of Fe_3C: Implications for carbon in the Earth's inner core, *Geophys. Res. Lett.*, *35*, L17306, doi:10.1029/2008GL034817.

Goldstein, J. L., and J. M. Short (1967a), Cooling rates of 27 iron and stony-iron meteorites, *Geochim. Cosmochim. Acta*, *31*(6), 1001–1023, doi:10.1016/0016-7037(67)90076-2.

Goldstein, J. L., and J. M. Short (1967b), The iron meteorites their thermal history and parent bodies, *Geochim. Cosmochim. Acta*, *31*(10), 1733–1770, doi:10.1016/0016-7037(67)90120-2.

Goncharov, A. F., J. Crowhurst, and J. M. Zaug (2004), Elastic and vibrational properties of cobalt to 120 GPa, *Phys. Rev. Lett.*, *92*(11), 115502, doi:10.1103/PhysRevLett.92.115502.

Hemley, R. J., and H. K. Mao (2001), In situ studies of iron under pressure: New windows on the Earth's core, *Int. Geol. Rev.*, *43*(1), 1–30.

Henriksson, K. O. E., N. Sandberg, and J. Wallenius (2008), Carbides in stainless steels: Results from ab initio investigations, *Appl. Phys. Lett.*, *93*, 191912, doi:10.1063/1.3026175.

Herbstein, F. H., and J. A. Snyman (1964), Identification of Eckstrom-Adcock iron carbide as Fe_7C_3, *Inorg. Chem.*, *3*(6), 894–896, doi:10.1021/ic50016a026.

Hillgren, V. J., C. K. Gessmann, and J. Li (2000), An experimental perspective on the light element in Earth's core, in *Origin of the Earth and Moon*, edited by Canup, R. M. and K. Righter, pp. 245–263, Univ. of Ariz. Press, Tucson.

Hirayama, Y., T. Fujii, and K. Kurita (1993), The melting relation of the system, iron and carbon at high pressure and its bearing on the early stage of the Earth, *Geophys. Res. Lett.*, *20*(19), 2095–2098, doi:10.1029/93GL02131.

Hofer, L. J. E., and E. M. Cohn (1959), Saturation magnetizations of iron carbides, *J. Am. Chem. Soc.*, *81*(7), 1576–1582, doi:10.1021/ja01516a016.

Huang, L., N. V. Skorodumova, A. B. Belonoshko, B. Johansson, and R. Ahuja (2005), Carbon in iron phases under high pressure, *Geophys. Res. Lett.*, *32*, L21314, doi:10.1029/2005GL024187.

Isaak, D. G., and O. L. Anderson (2003), Thermal expansivity of HCP iron at very high pressure and temperature, *Physica B*, *328*(3–4), 345–354, doi:10.1016/S0921-4526(02)01858-6.

Isaev, E. I., N. V. Skorodumova, R. Ahuja, Y. K. Vekilov, and B. Johansson (2007), Dynamical stability of Fe-H in the Earth's mantle and core regions, *Proc. Natl. Acad. Sci. U. S. A.*, *104*(22), 9168–9171, doi:10.1073/pnas.0609701104.

Jacobs, J. A. (1953), The Earth's inner core, *Nature*, *172*(4372), 297–298, doi:10.1038/172297a0.

Javoy, M., F. Pineau, and C. J. Allegre (1982), Carbon geodynamic cycle, *Nature*, *300*(5888), 171–173, doi:10.1038/300171a0.

Jephcoat, A., and P. Olson (1987), Is the inner core of the Earth pure iron?, *Nature*, *325*(6102), 332–335, doi:10.1038/325332a0.

Jiang, C., S. G. Srinivasan, A. Caro, and S. A. Maloy (2008), Structural, elastic, and electronic properties of Fe_3C from first principles, *J. Appl. Phys.*, *103*(4), 043502, doi:10.1063/1.2884529.

Kennett, B. L. N., E. R. Engdahl, and R. Buland (1995), Constraints on seismic velocities in the Earth from traveltimes, *Geophys. J. Int.*, *122*(1), 108–124, doi:10.1111/j.1365-246X.1995.tb03540.x.

Kohn, W., and L. J. Sham (1965), Self-consistent equations including exchange and correlation effects, *Phys. Rev.*, *140*(4A), A1133–A1138, doi:10.1103/PhysRev.140.A1133.

Kolorenč, J., and L. Mitas (2008), Quantum Monte Carlo calculations of structural properties of FeO under pressure, *Phys. Rev. Lett.*, *101*(18), 185502, doi:10.1103/PhysRevLett.101.185502.

Kresse, G., and J. Furthmuller (1996), Efficient iterative schemes for ab initio total-energy calculations using a plane-wave basis set, *Phys. Rev. B*, *54*(16), 11,169–11,186, doi:10.1103/PhysRevB.54.11169.

Kresse, G., and J. Hafner (1993), Ab initio molecular dynamics for liquid metals, *Phys. Rev. B*, *47*(1), 558–561, doi:10.1103/PhysRevB.47.558.

Kresse, G., and D. Joubert (1999), From ultrasoft pseudopotentials to the projector augmented-wave method, *Phys. Rev. B*, *59*(3), 1758–1775, doi:10.1103/PhysRevB.59.1758.

Kuneš, J., D. M. Korotin, M. A. Korotin, V. I. Anisimov, and P. Werner (2009), Pressure-driven metal-insulator transition in hematite from dynamical mean-field theory, *Phys. Rev. Lett.*, *102*(14), 146402, doi:10.1103/PhysRevLett.102.146402.

Kuramoto, K. (1997), Accretion, core formation, H and C evolution of the Earth and Mars, *Phys. Earth Planet. Inter.*, *100*(1–4), 3–20, doi:10.1016/S0031-9201(96)03227-X.

Li, J., and Y. Fei (2003), Experimental constraints on core compositions, in *Treatise on Geochemistry*, edited by Carlson, R. W., pp. 1–31, Elsevier, Amsterdam.

Li, J., H. K. Mao, Y. Fei, E. Gregoryanz, M. Eremets, and C. S. Zha (2002), Compression of Fe_3C to 30 GPa at room temperature, *Phys. Chem. Miner.*, *29*(3), 166–169, doi:10.1007/s00269-001-0224-4.

Lin, J. F., V. V. Struzhkin, H. K. Mao, R. J. Hemley, P. Chow, M. Y. Hu, and J. Li (2004), Magnetic transition in compressed Fe_3C from x-ray emission spectroscopy, *Phys. Rev. B*, *70*(21), 212405, doi:10.1103/PhysRevB.70.212405.

Lin, J. F., W. Sturhahn, J. Y. Zhao, G. Y. Shen, H. K. Mao, and R. J. Hemley (2005), Sound velocities of hot dense iron: Birch's law revisited, *Science*, *308*(5730), 1892–1894, doi:10.1126/science.1111724.

Lord, O. T., M. J. Walter, R. Dasgupta, D. Walker, and S. M. Clark (2009), Melting in the Fe-C system to 70 GPa, *Earth Planet. Sci. Lett.*, *284*(1–2), 157–167, doi:10.1016/j.epsl.2009.04.017.

Ma, Y. Z., M. Somayazulu, G. Y. Shen, H. K. Mao, J. F. Shu, and R. J. Hemley (2004), In situ X-ray diffraction studies of iron to Earth-core conditions, *Phys. Earth Planet. Inter.*, *143–144*, 455–467, doi:10.1016/j.pepi.2003.06.005.

Mao, H. K., Y. Wu, L. C. Chen, J. F. Shu, and A. P. Jephcoat (1990), Static compression of iron to 300 GPa and $Fe_{0.8}Ni_{0.2}$ alloy to 260 GPa: Implications for composition of the core, *J. Geophys. Res.*, *95*(B13), 21,737–21,742, doi:10.1029/JB095iB13p21737.

Mao, H. K., et al. (2001), Phonon density of states of iron up to 153 gigapascals, *Science*, *292*(5518), 914–916, doi:10.1126/science.1057670.

McDonough, W. F. (2003), Compositional model for the Earth's core, in *Treatise on Geochemistry*, edited by Carlson, R. W., pp. 547–568, Elsevier, Amsterdam.

Monkhorst, H. J., and J. D. Pack (1976), Special points for Brillouin-zone integrations, *Phys. Rev. B*, *13*(12), 5188–5192, doi:10.1103/PhysRevB.13.5188.

Mookherjee, M., and G. Steinle-Neumann (2009a), Detecting deeply subducted crust from the elasticity of hollandite, *Earth Planet. Sci. Lett.*, *288*(3–4), 349–358, doi:10.1016/j.epsl.2009.09.037.

Mookherjee, M., and G. Steinle-Neumann (2009b), Elasticity of phase-X at high pressure, *Geophys. Res. Lett.*, *36*, L08307, doi:10.1029/2009GL037782.

Mookherjee, M., and L. Stixrude (2009), Structure and elasticity of serpentine at high-pressure, *Earth Planet. Sci. Lett.*, *279*(1–2), 11–19, doi:10.1016/j.epsl.2008.12.018.

Morgan, J. W., and E. Anders (1980), Chemical composition of Earth, Venus, and Mercury, *Proc. Natl. Acad. Sci. U. S. A.*, *77*(12), 6973–6977, doi:10.1073/pnas.77.12.6973.

Nakajima, Y., E. Takahashi, T. Suzuki, and K. Funakoshi (2009), "Carbon in the core" revisited, *Phys. Earth Planet. Inter.*, *174*(1–4), 202–211, doi:10.1016/j.pepi.2008.05.014.

Nguyen, J. H., and N. C. Holmes (2004), Melting of iron at the physical conditions of the Earth's core, *Nature*, *427*(6972), 339–342, doi:10.1038/nature02248.

Nye, J. F. (1985), *Physical Properties of Crystals: Their Representation by Tensors and Matrices*, Oxford Univ. Press, Oxford, U. K.

Occelli, F., P. Loubeyre, and R. Letoullec (2003), Properties of diamond under hydrostatic pressures up to 140 GPa, *Nat. Mater.*, *2*(3), 151–154, doi:10.1038/nmat831.

Oganov, A. R., J. Brodholt, and G. D. Price (2002), Ab initio theory of phase transitions and thermoelasticity of minerals, in *EMU Notes in Mineralogy*, vol. 4, *Energy Modelling in Minerals*, edited by Gramaccioli, C. M., chap. 5, pp. 83–170, Eötvös Univ. Press, Budapest.

Ono, S., and K. Mibe (2010), Magnetic transition of iron carbide at high pressures, *Phys. Earth Planet. Inter.*, *180*(1–2), 1–6, doi:10.1016/j.pepi.2010.03.008.

Perdew, J. P., K. Burke, and M. Ernzerhof (1996), Generalized gradient approximation made simple, *Phys. Rev. Lett.*, *77*(18), 3865–3868, doi:10.1103/PhysRevLett.77.3865.

Poirier, J. P. (1994), Light elements in the Earth's outer core: A critical review, *Phys. Earth Planet. Inter.*, *85*(3–4), 319–337, doi:10.1016/0031-9201(94)90120-1.

Scott, H. P., Q. Williams, and E. Knittle (2001), Stability and equation of state of Fe_3C to 73 GPa: Implications for carbon in the Earth's core, *Geophys. Res. Lett.*, *28*(9), 1875–1878, doi:10.1029/2000GL012606.

Shabanova, I. N., and V. A. Trapeznikov (1973), Temperature dependence of the intensity of the characteristic energy losses of 2p electrons of iron in cementite, *J. Exp. Theor. Phys.*, *18*, 339–341.

Singh, S. C., M. A. J. Taylor, and J. P. Montagner (2000), On the presence of liquid in Earth's inner core, *Science*, *287*(5462), 2471–2474, doi:10.1126/science.287.5462.2471.

Skorodumova, N. V., R. Ahuja, and B. Johansson (2004), Influence of hydrogen on the stability of iron phases under pressure, *Geophys. Res. Lett.*, *31*, L08601, doi:10.1029/2004GL019736.

Sleep, N. H., and K. Zahnle (2001), Carbon dioxide cycling and implications for climate on ancient Earth, *J. Geophys. Res.*, *106*(E1), 1373–1399, doi:10.1029/2000JE001247.

Souriau, A., and P. Roudil (1995), Attenuation in the uppermost inner core from broad-band GEOSCOPE *PKP* data, *Geophys. J. Int.*, *123*(2), 572–587, doi:10.1111/j.1365-246X.1995.tb06872.x.

Steinle-Neumann, G. (2008), Magneto-elastic effects in compressed cobalt from first-principles, *Phys. Rev. B*, *77*(10), 104109, doi:10.1103/PhysRevB.77.104109.

Steinle-Neumann, G., L. Stixrude, and R. E. Cohen (1999), First-principles elastic constants for the hcp transition metals Fe, Co, and Re at high pressure, *Phys. Rev. B*, *60*(2), 791–799, doi:10.1103/PhysRevB.60.791.

Steinle-Neumann, G., L. Stixrude, R. E. Cohen, and O. Gulseren (2001), Elasticity of iron at the temperature of the Earth's inner core, *Nature*, *413*(6851), 57–60, doi:10.1038/35092536.

Steinle-Neumann, G., R. E. Cohen, and L. Stixrude (2004), Magnetism in iron as a function of pressure, *J. Phys. Condens. Matter*, *16*(14), S1109–S1119, doi:10.1088/0953-8984/16/14/020.

Stevenson, D. J. (1981), Models of the Earth's core, *Science*, *214*(4521), 611–619, doi:10.1126/science.214.4521.611.

Stixrude, L., and C. Lithgow-Bertelloni (2005), Thermodynamics of mantle minerals: I. Physical properties, *Geophys. J. Int.*, *162*(2), 610–632, doi:10.1111/j.1365-246X.2005.02642.x.

Stixrude, L., E. Wasserman, and R. E. Cohen (1997), Composition and temperature of Earth's inner core, *J. Geophys. Res.*, *102*(B11), 24,729–24,739, doi:10.1029/97JB02125.

Sturhahn, W., and J. M. Jackson (Eds.) (2007), Geophysical applications of nuclear resonant scattering, *Spec. Pap. Geol. Soc. Am.*, 421, 157–174.

Tajima, S., and S. Hirano (1990), Synthesis and magnetic properties of Fe_7C_3 particles with high-saturation magnetization, *Jpn. J. Appl. Phys. Part 1*, *29*(4), 662–668.

Tateno, S., K. Hirose, Y. Ohishi, and Y. Tatsumi (2010), The structure of iron in Earth's inner core, *Science*, *330*(6002), 359–361, doi:10.1126/science.1194662.

Terasaki, H., K. Nishida, Y. Shibazaki, T. Sakamaki, A. Suzuki, E. Ohtani, and T. Kikegawa (2010), Density measurements of Fe_3C liquid using X-ray absorption image up to 10 GPa and effect of light elements on compressibility of liquid iron, *J. Geophys. Res.*, *115*, B06207, doi:10.1029/2009JB006905.

Tsuzuki, A., S. Sago, S.-I. Hirano, and S. Naga (1984), High temperature and pressure preparation and properties of iron carbides Fe_7C_3 and Fe_3C, *J. Mater. Sci.*, *19*, 2513–2518.

Vočadlo, L., G. A. de Wijs, and G. Kresse (1997), First principles calculations on crystalline and liquid iron at Earth's core conditions, *Faraday Discuss.*, *106*, 205–218, doi:10.1039/a701628j.

Vočadlo, L., J. Brodholt, D. P. Dobson, K. S. Knight, W. G. Marshall, G. D. Price, and I. G. Wood (2002), The effect of ferromagnetism on the equation of state of Fe_3C studied by first-principles calculations, *Earth Planet. Sci. Lett.*, *203*(1), 567–575, doi:10.1016/S0012-821X(02)00839-7.

Wasson, J. T. (1985), *Meteorites: Their Record of Early Solar System History*, Freeman, New York.

Wood, B. J. (1993), Carbon in the core, *Earth Planet. Sci. Lett.*, *117*(3–4), 593–607, doi:10.1016/0012-821X(93)90105-I.

A. Chumakov, ID18 Nuclear Resonance Group, European Synchrotron Radiation Facility, Grenoble Cedex F-38043, France.

L. Dubrovinsky, K. Glazyrin, C. McCammon, M. Mookherjee, Y. Nakajima, and G. Steinle-Neumann, Bayerisches Geoinstitut, Universität Bayreuth, Bayreuth D-95440, Germany. (mainak.mookherjee@uni-bayreuth.de)

X. Wu, School of Earth and Space Sciences, Peking University, Beijing 100781, China.